Secrecy Analysis of Ambient Backscatter NOMA Systems under I/Q Imbalance

Xingwang Li, *Senior Member, IEEE,* Mengle Zhao, *Student Member, IEEE,* Yuanwei Liu, *Senior Member, IEEE,* Lihua Li, *Member, IEEE,* Zhiguo Ding, *Fellow, IEEE,* and Arumugam Nallanathan, *Fellow, IEEE*

***Abstract*—In this correspondence, we investigate the reliability and the security of the ambient backscatter (AmBC) non-orthogonal multiple access (NOMA) systems, where the source aims to communicate with two NOMA users in the presence of an eavesdropper. To be practical, we assume that all nodes and backscatter device (BD) suffer from in-phase and quadrature-phase imbalance (IQI). More specifically, some analytical expressions for the outage probability (OP) and the intercept probability (IP) are derived. In order to obtain more insights, the asymptotic behaviors for the OP in the high signal-to-noise ratio (SNR) regime are explored, and corresponding diversity orders are derived. Numerical results show that: 1) Although IQI reduces the reliability, it can enhance the security; 2) Compared with the orthogonal multiple access (OMA) systems, the considered AmBC NOMA systems can obtain better reliability when the SNR is lower; 3) There are error floors for the OP in the high SNR regime due to the reflection coefficient β; 4) There exists a trade-off between reliability and security.**

***Index Terms*—Ambient backscatter communication, in-phase and quadrature-phase imbalance, non-orthogonal multiple access, physical layer security**

I. Introduction

Non-orthogonal multiple access (NOMA) has been identified as one of the key technologies of the fifth-generation (5G) mobile networks since it has the advantages of high spectrum efficiency, massive connectivity and low latency [1], [2]. Different from orthogonal multiple access (OMA), the dominant feature of NOMA is to ensure multiple users to occupy the same frequency/time/code resources by power domain multiplexing. These advantages are achieved by employing superposed code (SC) at the transmitter and successive interference cancellation (SIC) at the receiver [3]. In addition, NOMA can ensure the fairness by allocating more power to the users with weak channel conditions [4].

On a parallel avenue, ambient backscatter communication (AmBC) is known as a potential technology with high spectrum- and energy-efficient for the green Internet-of-Things (IoT) and has attracted widespread attention in academia and industry [5]. In general, the AmBC system consists of three components: ambient radio-frequency (RF) source, backscatter device (BD) and reader. In this respect, the cooperative AmBC system was designed in [6] to allow the reader to recover information from both BD and RF source, and the closed-form analytical expressions for the bit error rate (BER) of optimal maximum-likelihood (ML) detector, suboptimal linear detector and SIC detector were derived. In [7], Guo *et al*. proposed a NOMA-assisted AmBC system to support massive BD connections. With the emphasis on the large intelligent surface (LIS), the authors in [8] studied the symbol error probability (SEP) performance of LIS-aided backscatter systems by considering both intelligent and random phase adjustments at the LIS reflectors.

Due to the broadcast characteristic of wireless communication environments, it is difficult to ensure secure communication for the wireless networks without being eavesdropped by the un-authored receivers. Physical layer security (PLS) has been proposed as an effective way to enhance the security of communication systems, which has sparked a great deal of research interests [9–11]. The authors of [9] investigated the reliability and the security of multi-relay networks in terms of the outage probability (OP) and the intercept probability (IP). Regarding NOMA systems, the authors proposed an enhanced security scheme to against full-duplex proactive eavesdropping [10]. To enhance the security of AmBC systems, the authors in [11] designed an optimal tag selection scheme of the multi-tag AmBC systems. However, the common characteristic of the above works are assumed that the transceiver RF front-ends are equipped with ideal components. Unfortunately, the practical RF components are prone to in-phase and quadrature-phase imbalance (IQI) due to mismatch and manufacturing non-idealities [12], [13], which limit the overall system performance. Therefore, it is of great practical significance to investigate the secrecy performance of the AmBC NOMA systems in the presence of IQI.

Although the PLS of the NOMA systems has been extensively studied, to the best of our knowledge, the impact of IQI on the PLS performance of the AmBC NOMA systems has not yet been investigated. This work aims to bridge this gap and investigate the effects of IQI on the PLS of the AmBC NOMA systems, where the eavesdropper can intercept the signals from both the source and the reflected signals from BD. Specifically, we study the reliability and the security by deriving the analytical expressions of the OP and the IP for the far user, the near user and the BD, respectively. Furthermore, to obtain more insights, the asymptotic behaviors for the OP

X. Li and M. Zhao are with the School of Physics and Electronic Information Engineering, Henan Polytechnic University, Jiaozuo, China (e-mail:lixingwangbupt@gmail.com, zhaomenglehpu@163.com).

Y. Liu and A. Nallanathanis are with the School of Electronic Engineering and Computer Science, Queen Mary University of London, London, UK, London, UK (email:{yuanwei.liu, a.nallanathan}@qmul.ac.uk).

L. Li is with the State Key Laboratory of Networking and Switching Technology, Beijing University of Posts and Telecommunications, China (email:lilihua@bupt.edu.cn).

Z. Ding is with the School of Electrical and Electronic Engineering, The University of Manchester, Manchester, UK (email: zhiguo.ding@manchester.ac.uk).

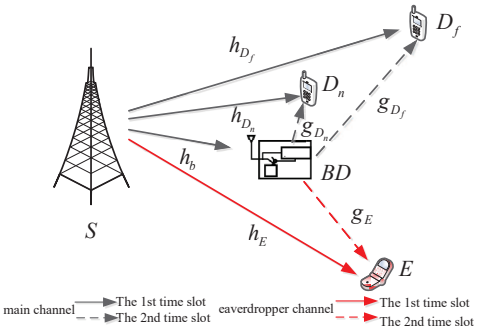

Fig. 1. System model

in the high signal-to-noise ratio (SNR) regime are explored, as well as the diversity orders. The results have shown that although IOI has deleterious effect on the reliability, it can enhance the secure performance of the considered system. Moreover, the proposed AmBC NOMA system can provide highly secure communication for the BD.

II. System Model

We consider a downlink AmBC NOMA system as illustrated in Fig. 1, which consists of one source (S), one BD, one far user (D_f), one near user (D_n) and one eavesdropper (E). We assume that: i) All the nodes are equipped with a single antenna; ii) The transceiver RF front-ends of the all nodes suffer from IQI. In addition, we have $h_{D_n} \sim \mathcal{CN}(0,\lambda_1)$, $h_{D_f} \sim \mathcal{CN}(0,\lambda_2)$, $h_E \sim \mathcal{CN}(0,\lambda_3)$, $g_{D_n} \sim \mathcal{CN}(0,\lambda_4)$, $g_{D_f} \sim \mathcal{CN}(0,\lambda_5)$, $g_E \sim \mathcal{CN}(0,\lambda_6)$. and $h_b \sim \mathcal{CN}(0,\lambda_7)$.

As in [12], IQI is modeled as phase and/or amplitude imbalance between the in-phase (I) and quadrature-phase (Q) branches. Thus, the baseband up-converted transmitted signals with IQI at S can be expressed as

$$x_{IQI} = \mu_{t_S} x_s + \nu_{t_S}(x_s)^*, \tag{1}$$

where $x_s = \sqrt{a_1 P_s}x_1 + \sqrt{a_2 P_s}x_2$, P_S is the transmit power at S; a_1 and a_2 are the power allocation coefficients for the near user and the far user with $a_1 + a_2 = 1$ and $a_1 < a_2$, respectively; x_1 and x_2 are the corresponding transmitted signals of D_n and D_f with $E\left(|x_1|^2\right) = E\left(|x_2|^2\right) = 1$, where $E(\cdot)$ and $(\cdot)^*$ are the expectation and conjugation operations, respectively. Moreover, $\mu_{t_s} = \frac{1}{2}\left(1 + \varsigma_t \exp\left(j\phi_t\right)\right)$, $\nu_{t_s} = \frac{1}{2}\left(1 - \varsigma_t \exp\left(-j\phi_t\right)\right)$, where ς_{t_s} and ϕ_{t_s} denote the TX amplitude and phase mismatch levels, respectively.

The BD backscatters the received signal to D_n with its own signal $c(t)$ with $E\left(|c(t)|^2\right) = 1$. Two types of received signals at i ($i \in \{D_n, D_f, E, \}$) are transmitted from S and backscattered from BD. Considering IQI at transceivers, the received signals at i can be expressed as

$$y_i = \mu_{r_i}\left\{\beta y_{BD} g_i\left[\mu_{t_{BD}} c(t) + \nu_{t_{BD}}(c(t))^*\right] + h_i x_{IQI} + n_i\right\} + \nu_{r_i}\left\{\beta y_{BD} g_i\left[\mu_{t_{BD}} c(t) + \nu_{t_{BD}}(c(t))^*\right] + h_i x_{IQI} + n_i\right\}^*, \tag{2}$$

where β is a complex reflection coefficient used to normalize $c(t)$; $n_i \sim \mathcal{CN}(0, N_0)$ is the complex additive white Gaussian noise (AWGN); h_i and g_i are the channel coefficients $S \to i$ and $BD \to i$, respectively; $\mu_{t_{BD}}$ and $\nu_{t_{BD}}$ represent the TX IQI coefficients of BD, with $\mu_{r_i} = \frac{1}{2}\left(1 + \varsigma_{r_i}\exp\left(-j\phi_{r_i}\right)\right)$, $\nu_{r_i} = \frac{1}{2}\left(1 - \varsigma_{r_i}\exp\left(j\phi_{r_i}\right)\right)$, ($i \in \{D_n, D_f, E, \}$), where ς_{r_i} and ϕ_{r_i} are the RX amplitude and phase mismatch levels, respectively. $y_{BD} = \mu_{r_{BD}} h_b x_{IQI} + \nu_{r_{BD}}(h_b x_{IQI})^*$ is the received signals at BD, where h_b is the channel coefficient of $S \to BD$.

Leveraging the NOMA protocol, D_f can decode the signals x_2, and D_n and E can decode signal x_2, x_1 and $c(t)$ in turn with the aid of SIC. Then, the received SINR of i ($i \in \{D_n, D_f, E\}$) can be given as[1]

$$\gamma_i^{x_2} = \frac{\xi_i a_2 \rho_i \gamma}{\rho_{g_i}\rho_b\left(A_i + Q_i\right)\gamma + \rho_i C_i \gamma + D_i}, \tag{3}$$

$$\gamma_i^{x_1} = \frac{\xi_i a_1 \rho_i \gamma}{\rho_{g_i}\rho_b(A_i + Q_i)\gamma + \rho_i(a_2 B_i + M_i)\gamma + D_i}, \tag{4}$$

$$\gamma_i^{c(t)} = \frac{Q_i \rho_{g_i}\rho_b \gamma}{\rho_{g_i}\rho_b A_i \gamma + \rho_i\left(B_i + M_i\right)\gamma + D_i}, \tag{5}$$

where $\gamma = P_s/N_0$ represents the transmit SNR at S; $\rho_i = |h_i|^2$, $\rho_{g_i} = |g_i|^2$, $\rho_b = |h_b|^2$, $\xi_i = |\mu_{r_i}|^2|\mu_{t_S}|^2 + |\nu_{r_i}|^2|\nu_{t_S}{}^*|^2$, $B_i = |\mu_{r_i}\mu_{t_S} - 1|^2 + |\nu_{r_i}|^2|\nu_{t_S}{}^*|^2$, $C_i = a_1\xi_i + M_i$, $D_i = |\mu_{r_i}|^2 + |\nu_{r_i}|^2$, $M_i = |\mu_{r_i}|^2|\nu_{t_S}|^2 + |\nu_{r_i}|^2|\mu_{t_S}{}^*|^2$, A_i and Q_i are provided at the top of the next page.

III. Performance Analysis

This section evaluates the reliability and the security of the AmBC NOMA systems by deriving the analytical expressions for the OP and the IP.[2] Moreover, we examine the asymptotic outage behaviors and the diversity orders in the high SNR region.

A. Outage Probability Analysis

1) Outage Probability for D_f

According to NOMA principle, the outage event occurs at D_f when D_f cannot successfully decode x_2. Thus, the OP at D_f can be given as

$$P_{out}^{D_f} = 1 - \mathrm{P}_r\left(\gamma_{D_f}^{x_2} > \gamma_{th2}\right), \tag{6}$$

where γ_{th2} is the target rate of D_f.

Theorem 1. *For Rayleigh fading channels, the analytical expression for the OP of the far user can be obtained as*[3]

$$P_{out}^{D_f} = 1 + \Delta_1 e^{\Delta_1 - \frac{D_{D_f} A_1}{\lambda_2 \gamma}}\mathrm{Ei}\left(-\Delta_1\right), \tag{7}$$

where $A_1 = \gamma_{th2}/\left(\xi_{D_f} a_2 - C_{D_f}\gamma_{th2}\right)$, $\Delta_1 = \lambda_2/\left(\lambda_7\lambda_5 A_1\left(A_{D_f} + Q_{D_f}\right)\right)$, and $\mathrm{Ei}(x) = \int_{-\infty}^{x}\frac{e^\rho}{\rho}d\rho$ is the exponential integral function [15].

[1]It should be pointed out that D_f only needs to decode its own signal x_2, that is, the SINR of D_f is $\gamma_{D_f}^{x_2}$.

[2]The reliability and security are another metrics to characterize the PLS of wireless communication systems without using any secrecy coding, which are formulated by the OP and the IP [14].

[3]The ideal and non-ideal results of OP and IP for the far user and near user can be written in a unified expression in (7), (9), (11), (12), (22) and (23).

$$A_i = |\mu_{r_i}|^2\beta^2|\mu_{r_{BD}}|^2|\nu_{t_{BD}}|^2\left(|\mu_{t_S}|^2+|\nu_{t_S}|^2\right)+|\mu_{r_i}|^2\beta^2|\nu_{r_{BD}}|^2|\nu_{t_{BD}}|^2\left(|\mu_{t_S}{}^*|^2+|\nu_{t_S}{}^*|^2\right)$$
$$+|\nu_{r_i}|^2\beta^2\left|\mu^*{}_{r_{BD}}\right|^2\left|\mu^*{}_{t_{BD}}\right|^2\left(|\mu_{t_S}{}^*|^2+|\nu_{t_S}{}^*|^2\right)+|\nu_{r_i}|^2\beta^2|\nu^*{}_{r_{BD}}|^2\left|\mu^*{}_{t_{BD}}\right|^2\left(|\mu_{t_S}|^2+|\nu_{t_S}|^2\right),$$

$$Q_i = |\mu_{r_i}|^2\beta^2|\mu_{r_{BD}}|^2|\mu_{t_{BD}}|^2\left(|\mu_{t_S}|^2+|\nu_{t_S}|^2\right)+|\mu_{r_i}|^2\beta^2|\nu_{r_{BD}}|^2|\mu_{t_{BD}}|^2\left(|\mu_{t_S}{}^*|^2+|\nu_{t_S}{}^*|^2\right)$$
$$+|\nu_{r_i}|^2\beta^2\left|\mu^*{}_{r_{BD}}\right|^2|\nu^*{}_{t_{BD}}|^2\left(|\mu_{t_S}{}^*|^2+|\nu_{t_S}{}^*|^2\right)+|\nu_{r_i}|^2\beta^2|\nu^*{}_{r_{BD}}|^2|\nu^*{}_{t_{BD}}|^2\left(|\mu_{t_S}|^2+|\nu_{t_S}|^2\right),$$

Proof: By substituting (3) into (6), the OP of D_f can be expressed as

$$P_{out}^{D_f}=\int_{A_1\left(\rho_{g_{D_f}}\rho_b\left(A_{D_f}+Q_{D_f}\right)+D_{D_f}\right)}^{\infty}f_{\rho_{D_f}}\int_0^{\infty}f_{\rho_{g_{D_f}}\rho_b}(y)dxdy$$
$$=\frac{2}{\lambda_7\lambda_5}\int_0^{\infty}e^{-\frac{A_1\left[y\left(A_{D_f}+Q_{D_f}\right)+D_{D_f}\right]}{\lambda_2}}K_0\left(2\sqrt{\frac{y}{\lambda_7\lambda_5}}\right)dy, \quad (8)$$

where $f_{\rho_{D_f}}=\frac{1}{\lambda_2}e^{-\frac{x}{\lambda_2}}$, $f_{\rho_{gD_f}\rho_b}(y)=\frac{2K_0\left(2\sqrt{\frac{y}{\lambda_7\lambda_5}}\right)}{\lambda_7\lambda_5}$, $K_0(x)$ is the modified Bessel function of the second kind. By using the integral equation [15, Eq. (6.614)], we can obtain (7) after some mathematical manipulations. ∎

Corollary 1. *At high SNRs the asymptotic expression for the OP of D_f of the AmBC NOMA system is given as*

$$P_{out,\infty}^{D_f}=1+\Delta_1 e^{\Delta_1}\mathrm{Ei}\left(-\Delta_1\right), \quad (9)$$

2) Outage Probability for D_n

To successfully decode x_1 at D_n, two conditions are needed to be met: 1) D_n can successfully decode x_2; 2) D_n can successfully decode its own information x_1. Therefore, the OP of D_n can be expressed as

$$P_{out}^{D_n}=1-\mathrm{P}_r\left(\gamma_{D_n}^{x_2}>\gamma_{th2},\gamma_{D_n}^{x_1}>\gamma_{th1}\right), \quad (10)$$

where γ_{th1} is the target rate of D_n.

Theorem 2. *For Rayleigh fading channels, the analytical expression for the OP of the near user can be obtained as*

$$P_{out}^{D_n}=1+\Delta_2 e^{\Delta_2-\frac{\varsigma D_{D_n}}{\lambda_1\gamma}}\mathrm{Ei}\left(-\Delta_2\right), \quad (11)$$

where $\varsigma=\max\left\{\frac{\gamma_{th1}}{\xi_{D_n}a_1-(a_2B_{D_n}+M_{D_n})\gamma_{th1}},\ \frac{\gamma_{th2}}{\xi_{D_n}a_2-C_{D_n}\gamma_{th2}}\right\}$, $\Delta_2=\frac{\lambda_1}{\lambda_7\lambda_4\varsigma(A_{D_n}+Q_{D_n})}$.

Proof: Following the similar derivation process of $P_{out}^{D_f}$, by substituting (3), (4) into (10), we can obtained $P_{out}^{D_n}$. ∎

Corollary 2. *At high SNRs the asymptotic expression for the OP of D_f of the AmBC NOMA system is given as*

$$P_{out,\infty}^{D_n}=1+\Delta_2 e^{\Delta_2}\mathrm{Ei}\left(-\Delta_2\right), \quad (12)$$

3) Outage Probability for BD

The BD signals can be successfully decoded when x_2 and x_1 are perfectly decoded at D_n. Thus, the OP of BD can be expressed as

$$P_{out}^{BD}=1-\mathrm{P}_r\left(\gamma_{D_n}^{x_2}>\gamma_{th2},\gamma_{D_n}^{x_1}>\gamma_{th1},\gamma_{D_n}^{c(t)}>\gamma_{thc}\right), \quad (13)$$

where γ_{thc} is the target rate for D_n decoding BD signals.

Theorem 3. *For Rayleigh fading channels, we have*

• *Ideal conditions ($\varsigma_t=\varsigma_r=1$, $\phi_t=\phi_r=0^\circ$)*

For ideal conditions, the analytical expression for the OP of the BD in (14) is provided at the top of next page.

where $\varsigma_{id}=\max\left\{\frac{\gamma_{th2}}{a_2-a_1\gamma_{th2}},\frac{\gamma_{th1}}{a_1}\right\}$, $\Delta_3=\frac{\lambda_1}{\lambda_7\lambda_4\varsigma_{id}\beta^2}$, $\vartheta_k=\cos\left[\frac{(2k-1)\pi}{2N}\right]$, *$N$ is an accuracy-complexity tradeoff parameter.*

• *Non-ideal conditions ($\varsigma_t=\varsigma_r\neq1$, $\phi_t=\phi_r\neq0^\circ$)*

For Non-ideal conditions, the analytical expression for the OP of the BD in (15) is provided at the top of next page.

where $\Delta_4=\frac{\lambda_1(B_{D_n}+M_{D_n})\gamma_{thc}}{\lambda_7\lambda_4(Q_{D_n}-A_{D_n}\gamma_{thc})}$, $\Delta_5=\frac{\lambda_1}{\lambda_7\lambda_4\varsigma(A_{D_n}+Q_{D_n})}$, $\Delta_6=\frac{D_{D_n}\gamma_{thc}}{(Q_{D_n}\gamma-A_{D_n}\gamma\gamma_{thc})}$, $\Delta_7=2\sqrt{\frac{(\vartheta_k+1)\Delta_6}{2\lambda_7\lambda_4}}$, $\Delta_8=\frac{\varsigma(A_{D_n}+Q_{D_n})(\vartheta_k+1)\Delta_6}{2\lambda_1\gamma}$.

Proof: For ideal conditions, substituting $\varsigma_t=\varsigma_r=1$ and $\phi_t=\phi_r=0^\circ$ into (3), (4), (5), then according to (13), $P_{out}^{BD,id}$ can be expressed as

$$P_{out}^{BD,id}=\int_{\frac{\gamma_{thc}}{\beta^2\gamma}}^{\infty}e^{-\frac{\varsigma_{id}\left(y\beta^2+1\right)}{\lambda_1}}\frac{2}{\lambda_7\lambda_4}K_0\left(2\sqrt{\frac{y}{\lambda_7\lambda_4}}\right)dy$$
$$=\underbrace{\int_0^{\infty}e^{-\frac{\varsigma_{id}\left(y\beta^2+1\right)}{\lambda_1}}\frac{2}{\lambda_7\lambda_4}K_0\left(2\sqrt{\frac{y}{\lambda_7\lambda_4}}\right)dy}_{a}$$
$$-\underbrace{\int_0^{\frac{\gamma_{thc}}{\beta^2\gamma}}e^{-\frac{\varsigma_{id}\left(y\beta^2+1\right)}{\lambda_1}}\frac{2}{\lambda_7\lambda_4}K_0\left(2\sqrt{\frac{y}{\lambda_7\lambda_4}}\right)dy}_{b}, \quad (16)$$

where b can be approximated by Gaussian-Chebyshev quadrature [16]. Utilizing [15, Eq. (6.611)] to calculate a, we can obtain the result of (14) after some mathematical manipulations. Similarly, $P_{out}^{BD,ni}$ can be obtained. ∎

Corollary 3. *At high SNRs the asymptotic expressions for the OP of the BD for the AmBC NOMA system can be given by*

• *Ideal conditions ($\varsigma_t=\varsigma_r=1$, $\phi_t=\phi_r=0^\circ$)*

$$P_{out,\infty}^{BD,id}=1+\Delta_3 e^{\Delta_3}\mathrm{Ei}\left(-\Delta_3\right), \quad (17)$$

$$P_{out}^{BD,id} = 1 + \Delta_3 e^{\Delta_3 - \frac{\varsigma_{id}}{\gamma\lambda_1}} \mathrm{Ei}\left(-\Delta_3\right) + \frac{\pi\gamma_{thc}}{N\beta^2\gamma\lambda_7\lambda_4} e^{-\frac{\varsigma_{id}}{\gamma\lambda_1}} \sum_{k=0}^{N} e^{-\frac{\gamma_{thc}(\vartheta_k+1)}{2\lambda_1}} K_0\left(2\sqrt{\frac{\gamma_{thc}\left(\vartheta_k+1\right)}{2\beta^2\gamma\lambda_7\lambda_4}}\right)\sqrt{1-\vartheta_k^2}, \tag{14}$$

$$\begin{aligned} P_{out}^{BD,ni} =& 1 - \Delta_4 e^{\frac{D_{D_n}}{\lambda_1\left(B_{D_n}+M_{D_n}\right)\gamma}+\Delta_4} \mathrm{Ei}\left(-\Delta_4\right) + \Delta_5 e^{\Delta_5 - \frac{\varsigma D_{D_n}}{\lambda_1}} \mathrm{Ei}\left(-\Delta_5\right) + e^{-\frac{\varsigma D_{D_n}}{\gamma\lambda_1}} \frac{\pi\Delta_6}{N\lambda_3\lambda_5} \sum_{k=0}^{N} e^{-\Delta_8} K_0\left(\Delta_7\right)\sqrt{1-\vartheta_k^2} \\ & - e^{\frac{D_{D_n}}{\lambda_1\left(B_{D_n}+M_{D_n}\right)\gamma}} \frac{\pi\Delta_6}{N\lambda_7\lambda_4} \sum_{k=0}^{N} e^{-\frac{D_{D_n}(\vartheta_k+1)}{2\lambda_1\left(B_{D_n}+M_{D_n}\right)\gamma}} K_0\left(\Delta_7\right)\sqrt{1-\vartheta_k^2}, \end{aligned} \tag{15}$$

• *Non-ideal conditions ($\varsigma_t = \varsigma_r \neq 1$, $\phi_t = \phi_r \neq 0°$)*

$$P_{out,\infty}^{BD,ni} = 1 - \Delta_4 e^{\Delta_4}\mathrm{Ei}\left(-\Delta_4\right) + \Delta_5 e^{\Delta_5}\mathrm{Ei}\left(-\Delta_5\right). \tag{18}$$

Next, to obtain more insights, the diversity orders for D_f, D_n and BD are investigated, which can be defined as:

$$d = -\lim_{\gamma\to\infty} \frac{\log\left(P_{out}^{\infty}\right)}{\log\gamma}, \tag{19}$$

Corollary 4. *The diversity orders of D_f, D_n and BD are given as:*

$$d_{D_f} = d_{D_n} = d_{BD}^{id} = d_{BD}^{ni} = 0. \tag{20}$$

Remark 1. *From **Corollary 1**, **Corollary 2**, **Corollary 3** and **Corollary 4**, we can see that when transmit SNR goes to infinity, the received SINR also grows into infinity, the asymptotic outage performance of the D_f, D_n and BD become a constant. It means that the OP exists error floors, which results in 0 diversity order. This error floor is determined by the parameters of IQI and the reflection coefficient β.*

B. Intercept Probability Analysis

User j ($j \in \{D_f, D_n, BD\}$) will be intercepted if E can successfully wiretap j's signal, i.e. $\gamma_E^p > \gamma_{thE,j}$, $p \in \{x_2, x_1, c\left(t\right)\}$. Thus, the IP of j by E can be expressed as

$$P_{int}^{j} = \mathrm{P}_r\left(\gamma_E^p > \gamma_{thE,j}\right), \tag{21}$$

where $\gamma_{thE,j}$ is the secrecy SNR threshold of j.

Theorem 4. *For Rayleigh fading channels, the analytical expressions for the IP of the far user, the near user and the BD can be respectively obtained as*

For the far user and the near user, we have

$$P_{int}^{D_f} = -\Delta_9 e^{\Delta_9 - \frac{D_E A_2}{\lambda_2\gamma}} \mathrm{Ei}\left(-\Delta_9\right), \tag{22}$$

$$P_{int}^{D_n} = -\Delta_{10} e^{\Delta_{10} - \frac{D_E\gamma_{thE1}}{\lambda_3\left(\left|\mu_{r_E}\right|^2\left|\mu_{t_s}\right|^2 a_1\gamma - \left(a_2 B_E + M_E\right)\gamma\gamma_{thE1}\right)}} \mathrm{Ei}\left(-\Delta_{10}\right), \tag{23}$$

where $\Delta_9 = \frac{\lambda_4}{\lambda_7\lambda_6 A_2\left(A_E+Q_E\right)}$, $A_2 = \frac{\gamma_{thE2}}{\xi_E a_2 - C_E\gamma_{thE2}}$, $\Delta_{10} = \frac{\lambda_3\left(\left|\mu_{r_E}\right|^2\left|\mu_{t_s}\right|^2 a_1 - \left(a_2 B_E + M_E\right)\gamma_{thE1}\right)}{\lambda_7\lambda_6\left(A_E+Q_E\right)\gamma_{thE1}}$.

For the BD, we have

• *Ideal conditions ($\varsigma_t = \varsigma_r = 1$, $\phi_t = \phi_r = 0°$)*

$$P_{int}^{BD,id} = 1 - \frac{\pi\gamma_{thE3}}{N\lambda_7\lambda_6\beta^2\gamma} \sum_{k=0}^{N} K_0\left(2\sqrt{\frac{\gamma_{thE3}\left(\vartheta_k+1\right)}{2\lambda_7\lambda_6\beta^2\gamma}}\right)\sqrt{1-\vartheta_k^2}, \tag{24}$$

• *Non-ideal conditions ($\varsigma_t = \varsigma_r \neq 1$, $\phi_t = \phi_r \neq 0°$)*

For Non-ideal conditions, the analytical expression for the IP of BD in (25) is at the top of next page.

where $\Delta_{11} = \frac{D_E\gamma_{thE3}}{\lambda_7\lambda_6\left(Q_E\gamma - A_E\gamma\gamma_{thE3}\right)}$, $\Delta_{12} = \frac{\lambda_3\left(B_E+M_E\right)\gamma_{thE3}}{\lambda_7\lambda_6\left(Q_E - A_E\gamma_{thE3}\right)}$, $\Delta_{13} = 2\sqrt{\frac{\Delta_{11}\left(\vartheta_k+1\right)}{2}}$.

Remark 2. *From **Theorem 4**, We can obtain that as the reflection coefficient β increases, both $P_{int}^{D_f}$ and $P_{int}^{D_n}$ decreases, while P_{int}^{BD} increases; Moreover, IQI parameters have beneficial effects on the IPs for the far user, the near user and the BD.*

IV. Numerical Results

This section provides some numerical results to validate the correctness of the analysis in Section III. The results are verified by using Monte Carlo simulations with 10^6 trials. Unless otherwise stated, we have the following settings: $N_0 = 1$, $\gamma_{thf} = 1$, $\gamma_{thn} = 2$, $\gamma_{thc} = 0.1$, $\gamma_{thE,D_n} = 1$, $\gamma_{thE,D_f} = 1.2$, $\gamma_{thE,BD} = 0.8$; The power allocation coefficients are $a_1 = 0.1$ and $a_2 = 0.9$; The channel fading parameters are $\lambda_1 = \lambda_3 = 1$, $\lambda_2 = 0.1$, $\lambda_4 = 0.5$, $\lambda_5 = 0.8$, $\lambda_6 = 0.2$, $\lambda_7 = 0.1$. The reflection coefficient is $\beta = 0.1$, while for the ideal RF front-ends, $\varsigma_t = \varsigma_r = 1$, $\phi_t = \phi_r = 0$.

Fig. 2 plots the OP and the IP versus the transmit SNR under ideal conditions and IQI with $\varsigma_t = \varsigma_r = \{1, 1.05\}$, $\phi_t = \phi_r = \{0°, 20°\}$. The theoretical results are in excellent agreements with the simulated results. A specific observation can be obtained that IQI has significant effect on the near user, which is negative for the OP and positive for the IP. This happens because the near user suffers from SIC, which is impaired by IQI. The changes of OP and IP for the BD are very obvious due to the effects of twice SICs impaired by IQI, which indicates that the BD performance is more sensitive to IQI in the high SNR regime. On the other hand, although IQI reduces the reliability of the considered system, it can enhance the security of the considered system. Specifically, when $SNR = 30dB$, the differences of the OP for D_f, D_n and BD between IQI and the ideal conditions are 0.00197, 0.03592 and 0.21261, respectively. This means that IQI can reduce the reliability of the considered system. When $SNR = 30dB$, the difference of the IP for BD between the ideal conditions and IQI is 0.22338; When $SNR = 10dB$, the differences of the IP for D_f and D_n between the ideal conditions and IQI are 0.00711 and 0.01448, respectively. This also reveals

$$P_{out}^{BD,ni} = 1 - \frac{\pi\Delta_{11}}{N}\sum_{k=0}^{N} K_0(\Delta_{13})\sqrt{1-\vartheta_k^2} + \Delta_{12}e^{\frac{D_E}{\lambda_3(B_E+M_E)\gamma}+\Delta_{12}}\mathrm{Ei}(-\Delta_{12}) + e^{\frac{D_E}{\lambda_3(B_E+M_E)\gamma}}\frac{\pi\Delta_{11}}{N}\sum_{k=0}^{N} e^{-\frac{D_E(\vartheta_k+1)}{2\lambda_3(B_E+M_E)\gamma}} K_0(\Delta_{13})\sqrt{1-\vartheta_k^2}, \quad (25)$$

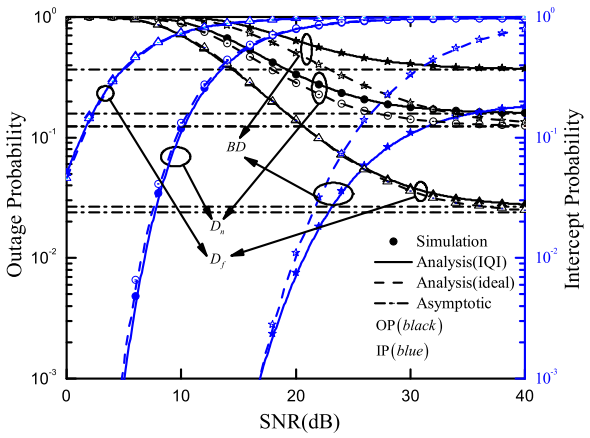

Fig. 2. OP and IP versus the transmit SNR

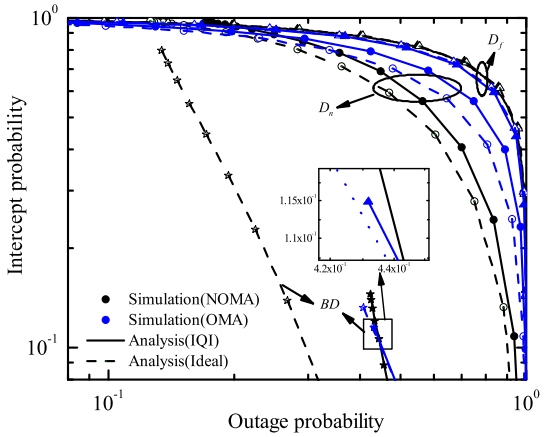

Fig. 3. IP versus OP for the D_f, D_n and BD

that IQI can enhance the security of the considered system. Moreover, it should be noted that when the SNR increases from 0dB to 40dB, the received SINR also increases. The effect of SINR on system performance is consistent with SNR, i.e., as the received SINRs at D_f, D_n and BD increase, the corresponding OPs and IPs decrease and increase, respectively. Finally, we can also see that there exists a trade-off between reliability and security, that is, when the outage performance is relaxed, the IP can be enhanced, and vice versa.

Fig. 3 demonstrates the impact of IP versus OP under ideal/non-ideal conditions with $\varsigma_t = \varsigma_r = \{1, 1.05\}$, $\phi_t = \phi_r = \{0°, 25°\}$. For the purpose of comparison, the curves of OMA are provided with $\gamma_{thc}^{OMA} = \gamma_{thE,BD}^{OMA} = 1.8$.[4] These results show that for a given OP, as IQI increases the corresponding IP increases, which leads the decrease of the secrecy performance. In addition, we can observe that the effect of IQI on each user is different. This effect depends on the decoding order of the users and the system parameter settings, where the far user is the least affected and experiences almost no performance degradation in the presence of IQI. BD changes are most significant. It can also be observed that for a given OP, the secure performance of NOMA is better than that of OMA system for the near user, the performance of the far user is the opposite. This is due to the large power allocation parameter of the far user. Finally, it should be noted that the IP of the BD is the smallest. This means that the BD has the best secure performance.

[4]The reason for this parameter setting is that when the parameter of NOMA is set to $\gamma_{thc}^{OMA} = \gamma_{thE,BD}^{OMA} = 1.8$, the OP of BD approaches to 1, and the IP is too small.

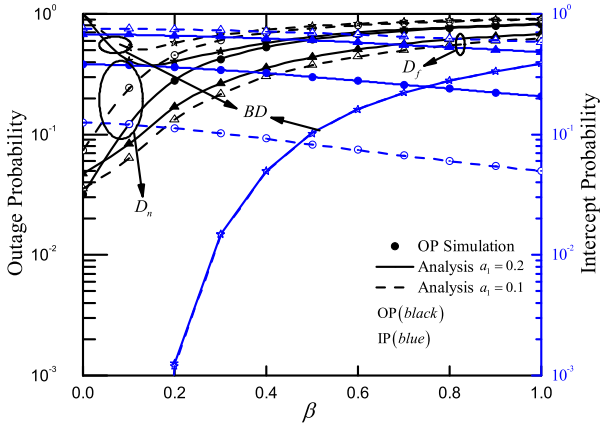

Fig. 4. OP and IP versus the reflection coefficient β for different power allocation parameter a_1

Fig. 4 presents the OP and the IP versus the reflection coefficient β for different power allocation parameters $a_1 = \{0.1, 0.2\}$ with $\varsigma_t = \varsigma_r = 1.1$, $\phi_t = \phi_r = 5°$, where the transmit SNRs for the OP and the IP are $SNR = 25dB$ and $SNR = 10dB$, respectively. From Fig. 4, we can observe that when β grows large, $P_{out}^{D_f}$ and $P_{out}^{D_n}$ increase, while $P_{int}^{D_f}$ and $P_{int}^{D_n}$ decrease. This happens because that when β becomes large, the interference of the backscatter link increases, which reduces the reliability of D_f and D_n, and enhances the security. The OP of BD first decreases and then increases as β increases. This happens because that when β is small, it is easier for D_n to decode its own information successfully, but

it is difficult to decode signals from BD. When β is large, it is difficult for D_n to decode its own information successfully. Noted that when $SNR = 25dB$, the outage performance is optimal when $\beta = 0.14$ for $a_1 = 0.2$, $\beta = 0.12$ for $a_1 = 0.1$. This means that the optimal reflection coefficient is determined by power allocation coefficient.

V. Conclusion

This paper investigates the impacts of IQI on the reliability and the security of the AmBC NOMA systems. This is carried out by deriving analytical expressions for the OP and the IP in the presence of IQI, and the asymptotic behaviors in the high SNR regime and diversity orders for the OP are analyzed. The simulation results show that although IQI reduces the reliability for the far user, the near user and the BD, it also enhances the security of the three devices. In addition, the increase of β will increase the OP and decrease the IP for far user and near user. Finally, we can conclude that the BD of the AmBC NOMA systems has better secrecy performance, which drives the application in the IoT networks.

References

[1] L. Bai, L. Zhu, T. Li, J. Choi, and W. Zhuang, "An Efficient Hybrid Transmission Method: Using Non-Orthogonal Multiple Access and Multiuser Diversity," *IEEE Trans. Veh. Technol.*, vol. 67, no. 3, pp. 2276–2288, Mar. 2018.

[2] L. Bai, L. Zhu, Q. Yu, J. Choi, and W. Zhuang, "Transmit Power-Minimization for Vector-Perturbation Based NOMA Systems: A Sub-Optimal Beamforming Approach," *IEEE Trans. Wireless Commun.*, vol. 18, no. 5, pp. 2679–2692, May 2019.

[3] X. Li, J. Li, Y. Liu, Z. Ding, and A. Nallanathan, "Residual Transceiver Hardware Impairments on Cooperative NOMA Networks," *IEEE Trans. Wireless Commun.*, vol. 19, no. 1, pp. 680–695, Jan. 2020.

[4] H. Liu, T. A. Tsiftsis, K. J. Kim, K. S. Kwak, and H. V. Poor, "Rate Splitting for Uplink NOMA with Enhanced Fairness and Outage Performance," *IEEE Trans. Wireless Commun.*, pp. 1–1, 2020.

[5] V. Liu, A. Parks, V. Talla, S. Gollakota, D. Wetherall, and J. R. Smith, "Ambient Backscatter: Wireless Communication out of Thin Air," *ACM SIGCOMM*, vol. 43, no. 4, pp. 39–50, Aug. 2013.

[6] G. Yang, Q. Zhang, and Y. Liang, "Cooperative Ambient Backscatter Communications for Green Internet-of-Things," *IEEE Internet Things J.*, vol. 5, no. 2, pp. 1116–1130, Apr. 2018.

[7] J. Guo, X. Zhou, S. Durrani, and H. Yanikomeroglu, "Design of Non-Orthogonal Multiple Access Enhanced Backscatter Communication," *IEEE Trans. Wireless Commun.*, vol. 17, no. 10, pp. 6837–6852, Oct. 2018.

[8] W. Zhao, G. Wang, S. Atapattu, T. A. Tsiftsis, and X. Ma, "Performance Analysis of Large Intelligent Surface Aided Backscatter Communication Systems," *IEEE Wireless Commun. Lett.*, pp. 1–1, 2020.

[9] X. Li, M. Huang, C. Zhang, D. Deng, K. M. Rabie, Y. Ding, and J. Du, "Security and Reliability Performance Analysis of Cooperative Multi-Relay Systems With Nonlinear Energy Harvesters and Hardware Impairments," *IEEE Access*, vol. 7, pp. 102 644–102 661, 2019.

[10] L. Lv, Z. Ding, J. Chen, and N. Al-Dhahir, "Design of Secure NOMA Against Full-Duplex Proactive Eavesdropping," *IEEE Wireless Commun. Lett.*, vol. 8, no. 4, pp. 1090–1094, Aug. 2019.

[11] Y. Zhang, F. Gao, L. Fan, X. Lei, and G. K. Karagiannidis, "Secure Communications for Multi-Tag Backscatter Systems," *IEEE Wireless Commun. Lett.*, vol. 8, no. 4, pp. 1146–1149, Aug. 2019.

[12] J. Li and M. Matthaiou and T. Svensson, "I/Q Imbalance in AF Dual-Hop Relaying: Performance Analysis in Nakagami-m Fading," *IEEE Trans. commun.*, vol. 62, no. 3, pp. 836–847, Mar. 2014.

[13] X. Li, M. Liu, C. Deng, P. T. Mathiopoulos, Z. Ding, and Y. Liu, "Full-Duplex Cooperative NOMA Relaying Systems With I/Q Imbalance and Imperfect SIC," *IEEE Wireless Commun. Lett.*, vol. 9, no. 1, pp. 17–20, Jan. 2020.

[14] Y. Zou, J. Zhu, X. Li, and L. Hanzo, "Relay selection for wireless communications against eavesdropping: a security-reliability trade-off perspective," *IEEE Netw.*, vol. 30, no. 5, pp. 74–79, Sep. 2016.

[15] I. S. Gradshteyn and I. M. Ryzhik, *Table of Integrals, Series, and Products*. New York, NY, USA: Academic Press, 2007.

[16] F. B. Hildebrand, *Introduction to numerical analysis*. New York, USA: Dover Publications, 1987.